

We are IntechOpen, the world's leading publisher of Open Access books Built by scientists, for scientists

4,800

Open access books available

122,000

International authors and editors

135M

Downloads

Our authors are among the

154

Countries delivered to

TOP 1%

most cited scientists

12.2%

Contributors from top 500 universities



WEB OF SCIENCE™

Selection of our books indexed in the Book Citation Index
in Web of Science™ Core Collection (BKCI)

Interested in publishing with us?
Contact book.department@intechopen.com

Numbers displayed above are based on latest data collected.
For more information visit www.intechopen.com



Microstructure and Property Co-relation of 4% Carbon Fe-C Alloy System

*Ranjan Kumar Behera, Sudipta Sen
and Subash Chandra Mishra*

Abstract

The suitable combination of strength and toughness makes ductile cast iron (DCI) the most preferred alloy for structural and engineering applications, among other members in the Fe-C alloy system. The property of DCI is dependent upon its microstructure that varies with dosage of alloying elements during the casting process as well as upon subjected to different heat treatment process. The microstructure of DCI consists of spheroidal graphite and either a single phase or combination of phases depending upon alloying element and heat treatment process, consequentially resulting in a combination of strength and toughness as desired for specified application. The current chapter discusses the relation between change in microstructural aspects with respect to various alloying elements as well as heat treatment processes. Emphasis is given on revealing the effect of physical characteristics with mechanical and tribological properties. The chapter is concluded by a case study on the effect of alloying elements and heat treatment processes on microstructure as well as mechanical and tribological properties of DCI.

Keywords: ductile cast iron, alloying, microconstituent, toughness, tribology

1. Introduction

The iron-carbon (Fe-C) system is a binary alloy system that comprises of 6.67% (max.) of carbon in iron, which is further classified into two alloys i.e., steel comprises of maximum 2% of C and cast iron having carbon that ranges from 2 to 6.67%. The cast iron is further classified into white cast iron and gray cast iron depending on the microstructure so obtained after the casting process. However the desired morphology to be obtained at room temperature can only be modified at the time of inoculation during the melting process by adding appropriate amount of alloying elements. Steel is the most preferable candidate for structural application as it possesses a good combination of strength, hardness, ductility, and impact toughness, whereas cast iron finds its application where the system is subjected to vibration such as base for heavy machinery installation. In structural application cast iron does not sit suitably due to its brittle nature that allows rapid fracture growth, having a high strength but low ductility and low impact toughness. The reason for such behavior is the nature of graphite in the final microstructure which

remains in the form of flakes with sharp edges that result in stress concentration sites upon loading and ultimately quicker crack propagation.

Spheroidal graphite cast iron (SGCI)/ductile cast iron (DCI) as the name suggests, has graphite in spherical form embedded in the matrix. The spherical shape is achieved by the addition of magnesium (Mg) and/or cerium (Ce) as inoculants, to the gray cast iron melt during the casting process. The graphite spheroids do not interfere with matrix continuity and eliminate the stress concentration effect that generates due to the presence of flaky graphite in case of gray cast iron, leading to improved ductility and impact toughness without affecting the strength and hardness. In addition, to these advantages, it possesses ease of castability, machinability and less cost of production. Because of these enhanced properties over the other cast irons, during the last five decades, the production and commercialization of SGCI have grown immensely. The versatility of SGCI in strength, toughness, tribological behavior and resistance to corrosion made it the preferable candidate for structural, automotive, agricultural and many more application including nuclear industry as well. Though in as-received form via melting and casting, it discloses desired property combination for the particular application, the properties can further be improved by employing suitable heat treatment techniques. The austempering heat treated ductile iron (referred as ADI) shows excellent combination of high strength and toughness [1, 2] along with better wear resistance [3, 4], excellent fatigue strength [5, 6] as well as fracture toughness [7, 8]. Application of suitable heat treatment process leads to transformation of as-cast ferritic or ferritic/pearlitic matrix into fully pearlitic, martensitic, and bainitic resulting variation in the properties. Among all the heat treatment processes employed the austempering treatment resulting in bainitic matrix is the most favorable member due to its strength, impact toughness, tribological behavior as well as fatigue and fracture toughness [9–13]. Tribological properties of austempered ductile iron (ADI) is observed to be in direct relationship with the austempering temperature and time. The consequences being increased hardness during the wear attributed to the fact that, the bainitic ferrite in the matrix undergoes strain hardening as it is less prone to thermal instability as compared to martensite [14]. On the other hand the tempering treatment with Boron alloyed DI reported to result in increased wear resistance; however, it decreases with increased boriding time [15]. Not only the matrix microstructure and alloying element is responsible for the wear behavior, but also as reported by Sugishita and Fujiyoshi [16]. Zimba et al. [17] the graphite characteristics viz. nodule size and distribution in the matrix has significant effect on the wear properties as well.

2. Effect of alloying element on morphological and mechanical properties of SGCI

To achieve desired properties for a particular application, control over matrix structure and morphological aspects is necessary, and that can be achieved by controlling processing parameters and the addition of alloying elements. The addition of alloying elements influences the mechanical properties by changing the cast matrix microstructure from ferritic to pearlitic, ferritic/pearlitic and/or austenitic depending upon the alloy composition. If the processing parameters such as tapping temperature and cooling rate are kept constant, the final matrix bends toward the matrix influencing element. Incorporation of Ni from 12 to 38% (max.), a highly ductile material of austenitic SGCI is obtained. On the other hand, a higher Si amount results in ferritic matrix and that of Cu and Mn lead to the formation of harder pearlitic matrix. A proper control of ferrite and pearlite influencing

elements results in a mixed ferritic/pearlitic structure having properties intermediate between ferritic and pearlitic grades of SGCI.

2.1 Effect of base composition

Silicon is the most vital element in the production of SGCI and influences the solidification process in conjunction with Carbon. An increase of 1% Si content shifts the eutectic composition toward the left (approximately 0.30% of carbon), resulting in low solidification temperature. With increasing Si content the eutectoid carbon content is lowered, and hence transformation occurs over a broadening range. **Figure 1(a)** depicts the inverse relationship of carbide content in the matrix with silicon content, and as disclosed with increased Si content there is a decrease in the carbide formation. Silicon is a graphitizer and ferrite promoter, hence reduces the strength properties of ferritic ductile iron, which if needed, further can be improved by the addition of desired amount of nickel. Increased silicon content increases the carbon equivalent (%CE), hence prevents the precipitation of carbides and allows the formation of more free form of carbon leading to increased nodule count (**Figure 1(b)**) and decreased hardness and UTS [18–20]. On the other hand, for austenitic grades increase in Si content increases the tensile strength and 0.2% yield strength [18]. The substantial influence of silicon on the ductile-brittle transition temperature of ferritic ductile iron is shown in **Figure 2** [21]. From **Figure 1**, it is clearly understood that to achieve optimum low-temperature toughness, the amount of Si should be maintained as low as possible. Fully ferritic carbide free ductile iron production needs high purity charge materials, proper holding and casting practice and highly effective inoculation for maximum nodule count. Higher amount of silicon leads to a reduction in low impact toughness, increased DBTT and decreased thermal conductivity. Si is held below 2.2% when producing the ferritic grades and between 2.5 and 2.8% when producing pearlitic grades [19, 20].

Manganese is a very strong carbide stabilizer at eutectoid graphitization and increases the amount of combined carbon. Excess Mn has little effect on solidification and only weakly retards primary graphitization. The presence of a correct amount of Mn forms manganese sulfide and reduces the proportion of combined carbon by removing the effect of sulfur [23]. Being a mild perlite promoter it results in increased hardness and proof stress but to a smaller extent. Manganese is added to the liquid melt to a limited amount as because it prevents the initiation of eutectoid transformation leading to lower rate of carbon diffusion in the ferrite and stabilizing cementite (Fe_3C). However, the noticeable problem with Mn addition is that

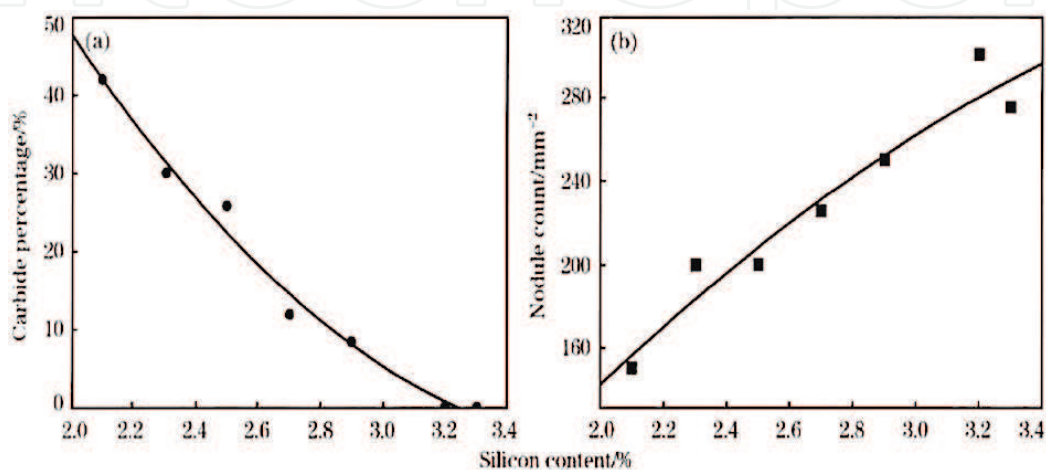


Figure 1.
Variation of carbide percentage (a) and nodule count (b) in ductile cast iron with silicon.

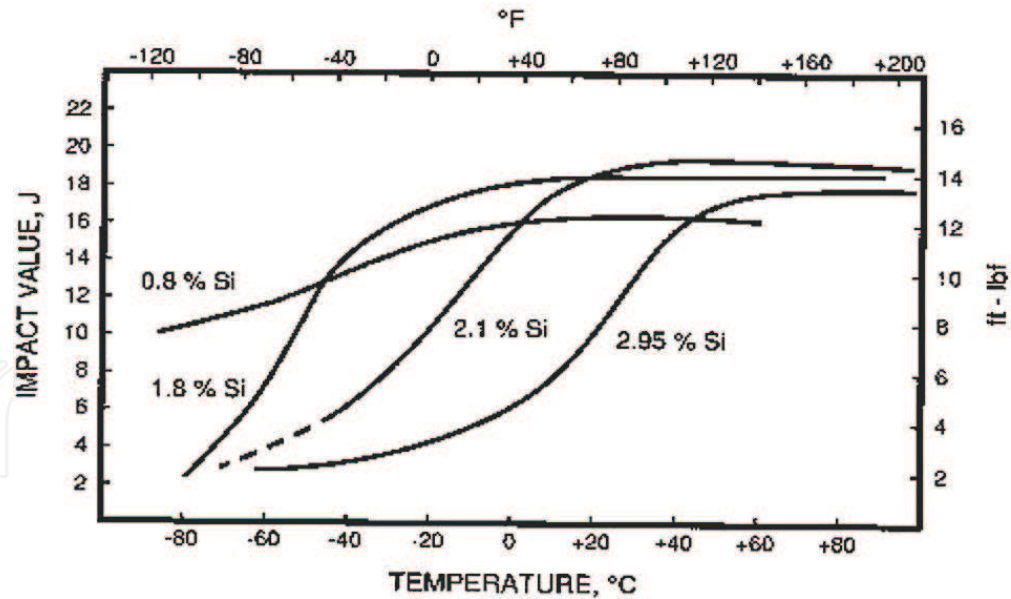


Figure 2. Influence of silicon content on the v-notched Charpy energy of ferritic ductile iron [22].

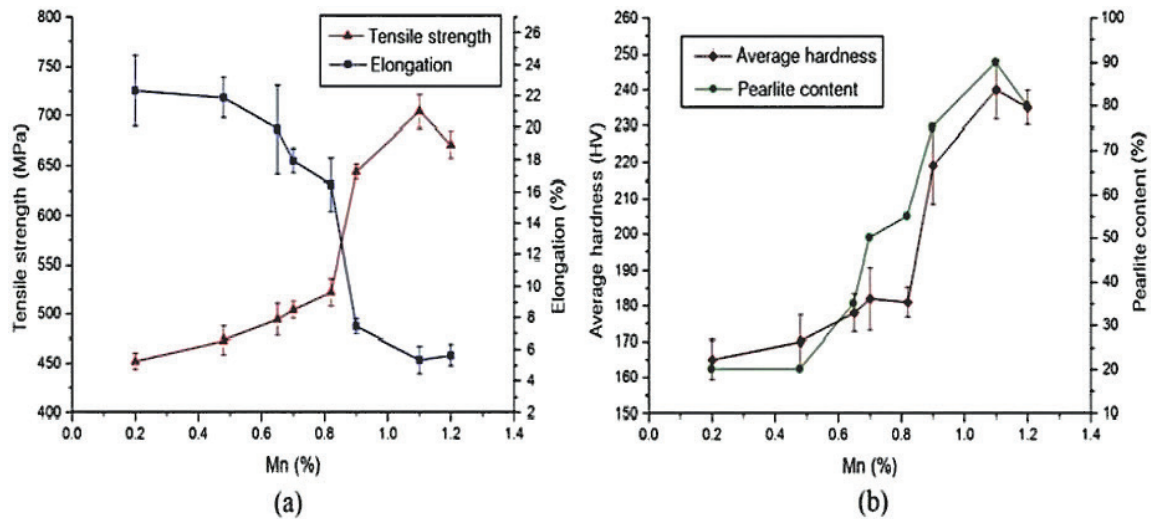


Figure 3. (a) The relationship between tensile strength and elongation versus Mn content (0.05% Cu), (b) average hardness and pearlite content versus Mn content (0.05% Cu) [27].

the embrittlement caused during the solidification process and hence limiting its range to (0.3–1.01) [24–26]. Mn is held between 0.4 and 0.6% when making pearlitic grades and below 0.3% when making ferritic grades and can be achieved by dilution with high purity pig iron to avoid pearlite and carbide formation [25, 26]. Higher Mn content leads to increased pearlite content resulting in increased strength and hardness and decreased Si elongation, **Figure 3**. However for a ferritic grade of SGCI Mn dissolved into the ferrite matrix and improves strength [27]. Use of higher Mn level is not preferred as it causes segregation at the grain boundaries that causes grain boundary carburet and creation of secondary phase along the boundaries leading to degradation in plasticity in SG cast iron. In combination with Ni, higher manganese content can stabilize austenite and increases carbide by depressing the solidification cooling curve encouraging graphite to segregate at a lower temperature consequentially resulting lower generation of free graphite and reduced ductility and impact toughness [28–31].

Sulfur affects the form of carbon in a manner which is opposite to that of Si. The higher the S content, the higher will be the amount of combined carbon, thus tends to form a hard and brittle matrix. An excessive amount of S will increase the tendency of gross defects above 0.015% promote the formation of quasi-flaky graphite [23, 26]. The addition of S is done for better machinability, but it is kept around 0.009, and maximum 0.015% as the larger additions of Sulfur may cause the hot (red) shortness [24]. Sulfur is an active interfacial element and has less solid solubility in austenite, therefore, gets enriched in liquid melt and at the freezing point. The presence of S encourages the eutectic graphite to branch frequently resulting in formation of chunky graphite [32].

Phosphorus combines with iron to form iron phosphide and produces a ternary eutectic with cementite and austenite. The ternary eutectic is known as steadite, which is relatively brittle and tends to form a continuous network outlining the primary austenite dendrites resulting lower toughness. It increases fluidity and extends the range of eutectic freezing, thus increasing primary graphitization when Si content is high. Incorporation of P above 0.05% can produce internal defects. It also causes embrittlement of iron, increases the ductile-brittle transition temperature, promotes galvanizing and temper-embrittlement. P often segregates to grain boundaries and produces carbide/phosphide complexes, hence needs to be maintained as low as possible. P is kept intentionally low as it causes cold shortness and so the property of ductile iron will be ruined [24].

Magnesium is used as nodulizer and responsible for spherical form of graphite, but at lower level chunky graphites are formed. Like sulfur, it is also an interfacial element and has less solid solubility in austenite. Magnesium makes the eutectic graphite grow with screw dislocations along the crystal orientation, giving the eutectic graphite growth characteristic into a spherical form. The lower level of Mg counteracts the surface activity of sulfur and oxygen promoting the formation and growth of chunky graphite particles. Due to the segregation effect when Magnesium content becomes high enough the graphite shape converts to spherical form [32].

2.2 Effect of alloying element

Chromium prevents the corrosion by forming the layer of chromium oxide on the surface and stops the further exposition of the surface to the atmosphere. However, as it is a strong carbide former, it is not required in carbide free structure. In general it is kept around 0.05%. It must be kept <1% in GGG-50 grade [24].

Nickel is used for strengthening ferrite in addition to Si leading to increased UTS without compensating ductility and impact values. It is usually added in traces due to high cost and also to avoid the embrittlement of matrix (if it exceeds 2%) [24]. Increased Ni content decreases the ductility for austenitic grade SGCI [33]. Nickel assists in shifting the transformation temperature boundary leading to attention of desired phase at lower temperature when alloyed with Ni as compared to that for an alloy without Ni. Additionally it has the ability to prevent the precipitation of secondary carbides in the final microstructure. Uma et al. [34] studied the effect of toughened austempered SG cast iron with increasing Ni content up to 2.5%. It is reported in their work that, with increasing Ni content pearlite content is increased in the as-cast matrix. Also, the retained austenite gets stabilized in the final microstructure. It is increased due to the fact that Ni concentrates in the austenite phase in the ($\alpha + \gamma$) region, resulting in increased impact toughness and wear resistance. When subjected to austempering treatment SG cast iron with Ni content higher than 0.5%, slows down the bainitic reaction and causes the formation of martensite at the austenite cell boundaries on cooling [32]. Although the addition

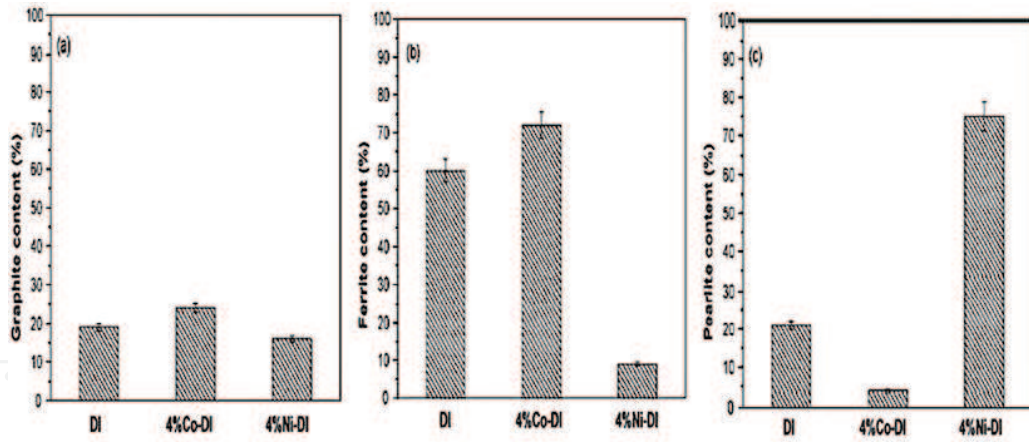


Figure 4. Comparison of constituent content in the microstructure of the Co and Ni alloyed SG cast irons: (a) graphite, (b) ferrite and (c) pearlite [35].

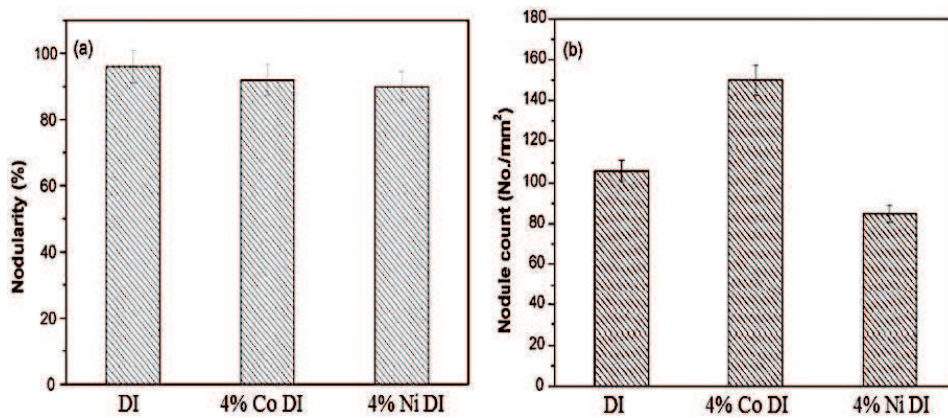


Figure 5. Comparison of nodular graphite of the Co and Ni alloyed SG cast irons: (a) nodularity and (b) nodule count [35].

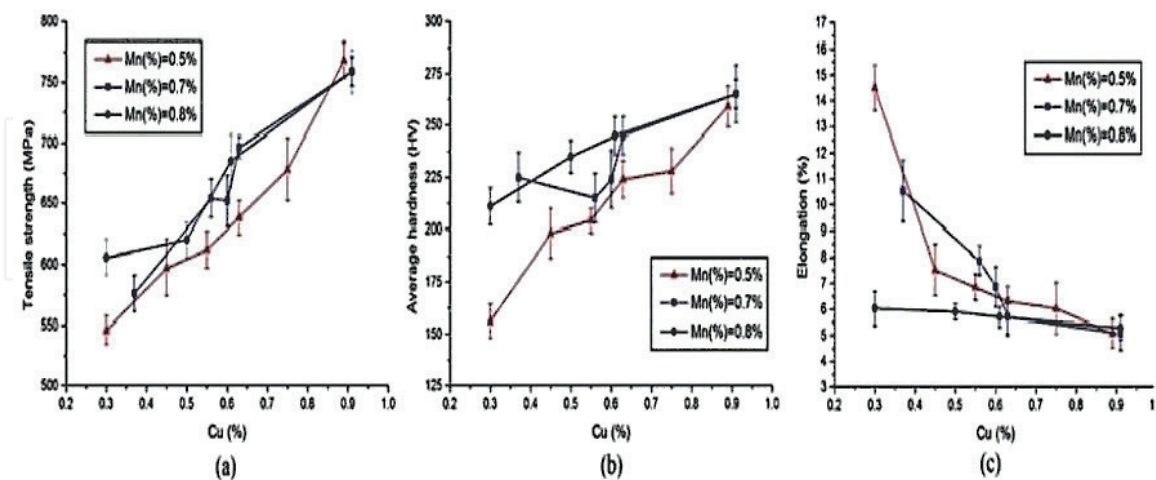


Figure 6. Relationship between the mechanical properties and the copper content for different Mn level [27]. (a) Mn content vs. Tensile Strength, (b) Mn content vs. Average Hardness, (c) Mn content vs. % Elongation.

of Ni promotes the stabilization of austenitic matrix in SG cast iron, it accelerates the formation of pearlite by shifting the knee of transformation diagram to higher time intervals. Thus, the eutectoid transformation of ductile cast iron in cooling austenite has resulted in a significant amount of pearlite structure (Figure 4) and

decreasing nodularity and nodule count (**Figure 5**) with increased yield and tensile strength and hardness with decreased ductility as well as impact toughness [35].

Copper is a strong pearlite promoter and is undesirable in ferritic grade. It increases the UTS, 0.2% yield strength and hardness (**Figure 6**) without an embrittlement in the matrix. In total Cu is kept between 0.4–0.8% [24, 25]. Along with promoting, it also refines the slice distance of pearlite in the eutectoid transformation period and is beneficial in stabilizing super-cooled austenite and increases the closing rate of the austenite shell that enables graphite to achieve perfectly spherical shape [27, 32, 36]. Copper strengthens the matrix when Mn levels are low. Unlike Mn, copper has an adverse effect on segregation and usually gathers at the interface between graphite and matrix. As a result, the diffusion of C is restricted due to a higher concentration of Cu, which leads to the formation of perfectly spherical nodules and increased nodule count. The combined effect of Cu and Ni, when subjected to austempering treatment, balances the hardenability, segregation tendency of Mn and inhibits the transformation of untransformed austenite into pearlite during quenching to austempering temperature. An excess amount of Cu results in the evolution of copper or copper-rich phase that affects the mechanical properties [37].

Molybdenum is a mild pearlite promoter and forms intercellular carbides especially in heavy sections leading to increased proof stress and hardness and also improves properties at elevated temperature [24]. Also, Mo segregates at the grain boundaries causing decrease in impact toughness. When subjected to austempering or ausforming process increased amount of Molybdenum stabilizes and increases austenite and bainite content. At zero Mo content the matrix is mainly bainitic, but with the increased amount it also increases the amount of carbide [18]. Mo, with an extreme tendency of segregating to the last solidification area, retards the bainite reaction and causes the micro shrinkage porosity in the intercellular region. Consequently, the Mo alloyed iron offers the lowest impact strength [21].

Rare earth (RE) materials in the nodulizer can eliminate the bad effect of the interferential elements like titanium, bismuth, arsenic, antimony, etc. and reduce the content of Si and Mg, which is helpful to avoid graphite degeneration. Ferro et al. [38] in their work reported that the graphite structure and nodule count can be improved by a well-dosed amount of RE elements in the inoculant composition. This is caused by a large decrement in surface free energy at liquid/graphite interface due to adsorption on graphite. RE elements also favor the graphite shape due to their neutralization effect of excesses of contaminants which cause nodule degeneration. However excess RE metals may cause graphite deterioration, especially in heavy castings where they form microsegregation at grain boundaries, which can be neutralized by proper addition of Bismuth. In another work by Choi et al. [39] it was reported that addition of rare earth elements influences the formation of ferrite at the vicinity of graphite nodules. The addition of RE increases the ferrite thickness with increased casting thickness due to slower cooling rate than that of castings without RE. However, in the case of thicker casting (40 mm), it does not play any significant role on ferrite formation. Also increasing RE up to 0.02% there was a reduction in nodule size and the nodule size increases with increasing RE from 0.02 to 0.03%. However, the graphite nodule size is further decreased when the RE content is again increased to 0.04%. Furthermore, the presence of RE changes nucleation and growth rate by changing the liquid's temperature. The addition of RE appears to increase undercooling, as a result of which its nucleation rate is increased, but the growth rate is decreased. Rare earth elements like lanthanum increases nodule count with increasing content when La to S ratio is as low as 1, hence increases the strength and ductility. However, it does not show any significant development in the nodularity value, which remains almost constant with increasing La amount [21].

3. Case study

3.1 Experimental details

3.1.1 Specimen preparation

In our study to investigate the structure–property relationship, ductile iron test blocks were prepared with different alloying elements and chemical composition by weight percentage is presented in **Table 1**. To investigate the mechanical and tribological properties specimens of $25 \times 10 \times 5 \text{ mm}^3$ were machined from the test block and then austenitized at 1000°C for 90 min followed by quenched in $\text{KNO}_3 + \text{NaNO}_3$ (1:1 ratio) at 500°C . The specimens were kept in the salt solution at 500°C for 4 h so as to obtain complete transformation of as-cast matrix. Post quenching the specimens were cooled to room temperature via air cooling, followed by the oxide layer formed on specimen surface was removed by conventional filing and emery paper polishing method.

3.1.2 Vickers hardness and wear testing

The as-cast and austempered specimens are subjected to hardness measurement with the help of a Vickers hardness tester by applying 20 kg load and keeping indenter on the surface for 10 s. Tribological properties were investigated by employing wear test on Ducom TR-208-M1 Ball on plate type wear tester consisting of a 0.4 mm spherical tipped diamond cone indenter of 120° angle. The wear test was conducted at 3 different loads of 10, 20 and 30 N and the travel distance being 7.54 m at a linear velocity of 0.063 m/s. The weights for corresponding specimens before and after test was measured with the help of electronic balance with 0.1 mg accuracy, and prior to the weight measurement specimens were cleaned ultrasonically with acetone before and after the wear took place.

The working principle for ball on plate wear tester is very much similar to that of pin on disc equipment. The only difference between both of the equipment is, the specimen in the pin on disc is in the form of cylindrical pin and the disc on the counterpart rotates against it, where the load is applied on the specimen end. On the

Elements	Wt. %	
	Alloy 1	Alloy 2
C	3.45	3.61
Si	2.07	2.1
Mn	0.15	0.2
S	0.008	0.007
P	0.024	0.022
Cr	0.02	0.03
Ni	0.15	0.47
Cu	—	0.009
Mo	—	0.001
Mg	0.043	0.043
Ce	—	0.004
Fe	Balance	Balance

Table 1.
Chemical composition of specimens in wt.%.

other hand, in case of ball on plate the specimen is fixed on the rotating plate and the indenter being fixed as well as load is applied on this end.

3.1.3 Microstructural and wear morphology characterization

To understand the wear behavior of respective as-cast and austempered specimens' morphological examination was carried out for microstructural aspects. The specimens were initially underwent rough polishing using belt polisher followed by semi finishing polish with 1/0, 2/0, 3/0, 4/0 grades of emery paper and alumina slurry polishing using cloth polisher. The final polishing was carried out using 1 μm diamond paste with the help of cloth polisher. The specimens were observed under microscope in unetched condition to investigate the graphite morphology and distribution in respective a-cast and austempered specimens. And after that each specimen was etched with 2% Nital solution and observed under microscope to obtain the phase characteristics and distribution in the matrix. Additionally the as-cast and austempered specimens subjected to X-ray diffraction investigation for detection of any impurity or precipitation resulted during casting or heat treatment process.

The worn surfaces of respective as-cast and heat treated specimens for both the alloys were observed under optical microscope after the tribology test. The worn surfaces also observed under FESEM and EDAX to understand the wear phenomena and the presence of any foreign element contributing toward the tribological behavior.

3.2 Results and discussion

3.2.1 Morphological characterization

The XRD investigation, **Figure 7**, revealed that there is no trace of any kind of residual phases or precipitation of any impurity present in the final microstructure. It was noticed that only BCC crystallographic planes (110), (200) and (211) are present in the as-cast specimen (**Figure 7(a)**) justifying ferrite and pearlite matrix. On the other hand BCC (110) and (211) and FCC (311) planes were observed for austempered specimens (**Figure 7(b)**) justifying bainitic matrix that is a combination of austenite and ferrite resulted due to the quenching and cooling processes in salt solution and ambient air respectively. The quantitative analysis shows higher carbon content as well as austenite volume fraction for Alloy 2 resulted due to the present of significantly higher amount of Ni as compared to Alloy 1, which act as austenite promoter during the austenitization stage and also helps in retaining the phase during the transformation process to the room temperature microstructure [40].

The microstructures of as-cast and austempered specimens for Alloy 1 and Alloy 2 were illustrated in **Figure 8**. The as-cast matrix of Alloy 1 (**Figure 8(a)**) appeared to have a mixture of ferrite, the white areas around graphite nodules and pearlite, the black area surrounding the white ferrite area in nature. This structure is referred as bull's eye ferritic/pearlitic one with graphite nodules surrounded by ferrite. On the other hand, microstructure of Alloy 2 (**Figure 8(b)**) has fully ferritic in nature surrounding the graphite globules. The difference is attributed to higher amount of Si content which is a strong ferrite promoter [41]. **Figure 8(c)** shows the coarse upper bainitic microstructure resulted by austempered heat treatment process. Quantitative metallographic analysis illustrates that nodularity (roundness of graphite particles) is above 90% that belongs to the Grade I nodularity, for both as-cast and heat treated specimens in both the alloys. The graphite characteristic (nodularity) and distribution (nodule count) for respective alloys in as-cast as well as austempered condition is presented in **Table 2**. It can be observed that Alloy 1 has less no. of nodules than Alloy 2, resulted due to lower Si content and additional Ce

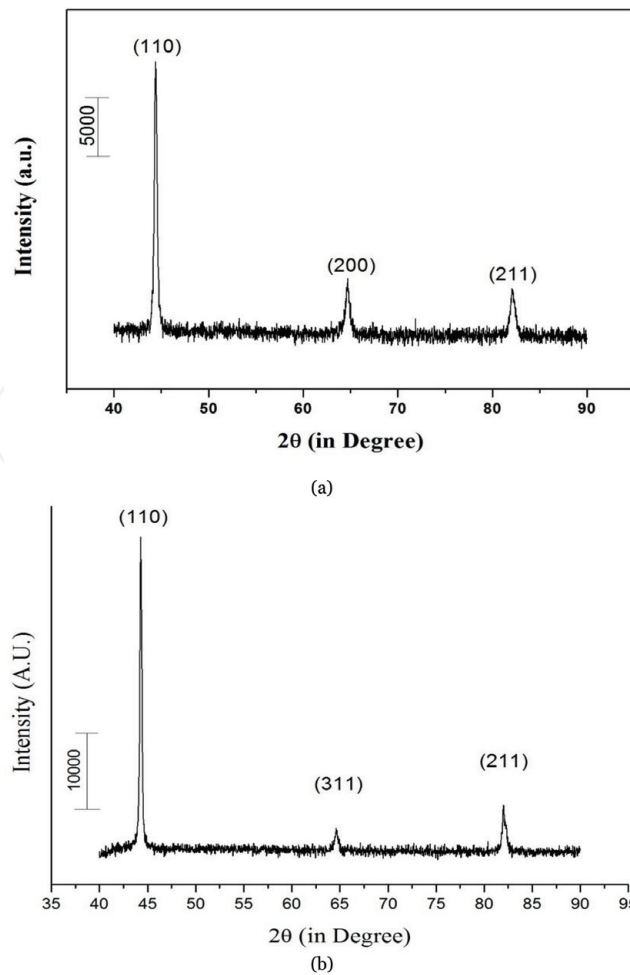


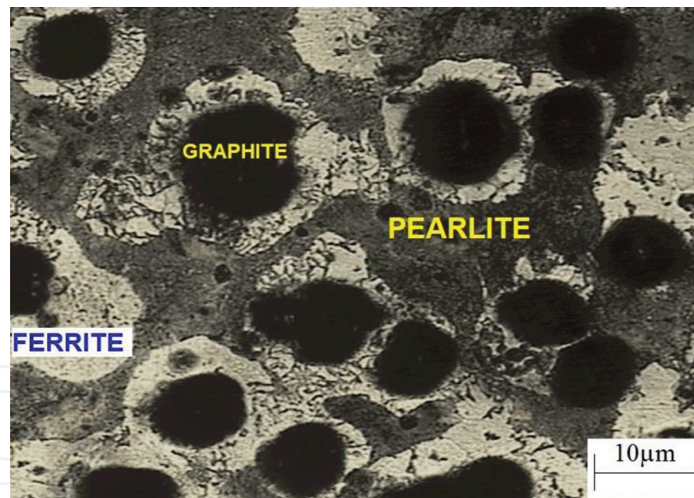
Figure 7. X-ray diffraction pattern for respective specimens. (a) As-cast and (b) austempered.

as well as higher Ni content in the latter case [42, 43]. The quantitative analysis also reveals the higher bainite volume fraction for Alloy 2 as a consequence of higher Ni content, as was observed from quantitative X-ray diffraction analysis.

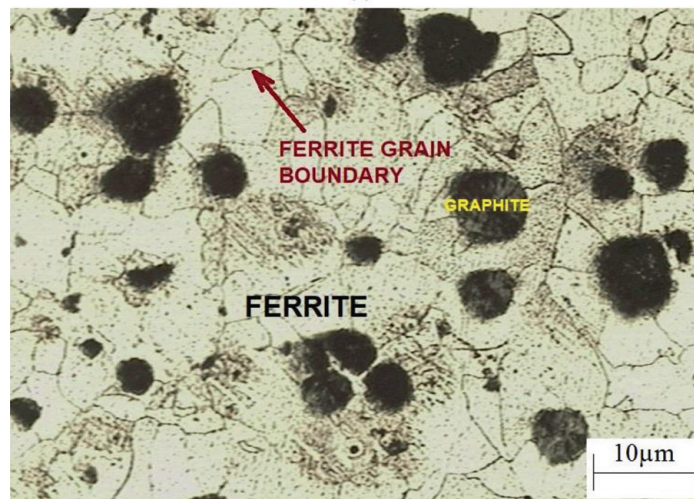
3.2.2 Hardness and wear system response

The Vickers hardness value for the as-cast and austempered specimens of both Alloy 1 and Alloy 2 are presented in **Figure 9**. The hardness was found to be higher for austempered specimen with upper bainitic matrix as compared to the as-cast ferritic and ferritic + pearlitic specimens. Alloy 1 has higher hardness in as-cast condition as compared to Alloy 2 which is credited to the amount of pearlite in the matrix, whereas Alloy 2 has only ferritic matrix in nature. On the other hand the case is reverse for austempering treated specimens, i.e., Alloy 2 has higher hardness value than Alloy 1 because of higher amount of Ni in the former resulting combination of higher amount of austenite and eutectoid ferrite in the matrix.

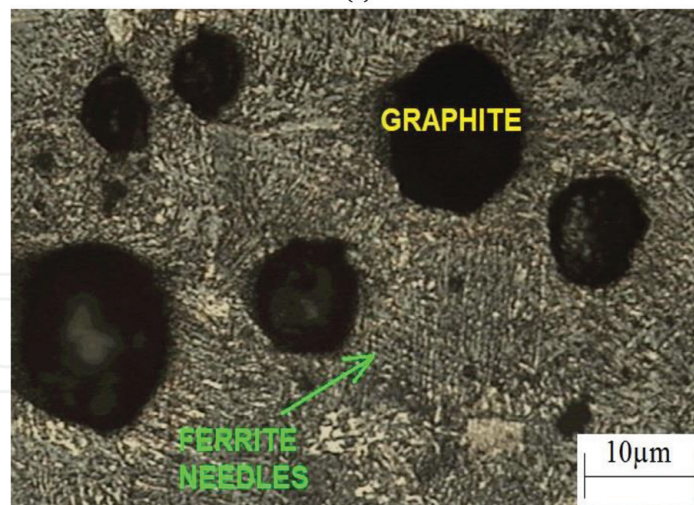
The wear system appears to have resulted in variation of weight loss/gain with variation of applied load for respective as-cast and austempered specimens and decreases continuously for as-cast specimen when load was increased from 10 to 20 N. On the contrary upon increase in load to 30 N a gain was observed which might be due to hardening of surface when operating under repeated no. of cycles. On the other hand, weight gain was observed for austempered specimens when operating under 20 and 30 N. On comparing with hardness values for respective specimens the weight loss at 10 N was observed to be lowest for the specimen with higher hardness value consequence of pearlite in the matrix [44]. The effect of



(a)



(b)



(c)

Figure 8. Microstructure of as-cast and austempered specimens. (a) As-cast matrix for Alloy 1, (b) as-cast matrix for Alloy 2, and (c) austempered matrix for both Alloy 1 and Alloy 2.

matrix was appeared to have direct effect on the wear rate, where the hardness was higher for bainitic matrix and the wear rate is less as compared to the ferritic and ferritic/pearlitic specimens with lower hardness with higher rate of wear. At 20 N load upper bainitic matrix showed a marginal gain in weight, but as-cast specimen had significantly lose some weight. Further at 30 N again weight gain was observed for both austempered and as-cast specimen.

Alloy	Heat treatment	Nodularity (in %)	Nodule count (mm ⁻²)	Phase volume fraction (in %)		Carbon content in austenite
				Austenite	Ferrite	
Alloy 1	As-cast	92	28	—	—	—
Alloy 2		95	33	—	—	—
Alloy 1	Austempered	91	43	70.00%	30.00%	2.5387
Alloy 2		93	50	88.51%	11.49%	2.5941

Table 2.
Microconstituents of as-cast and austempered specimens of respective alloys.

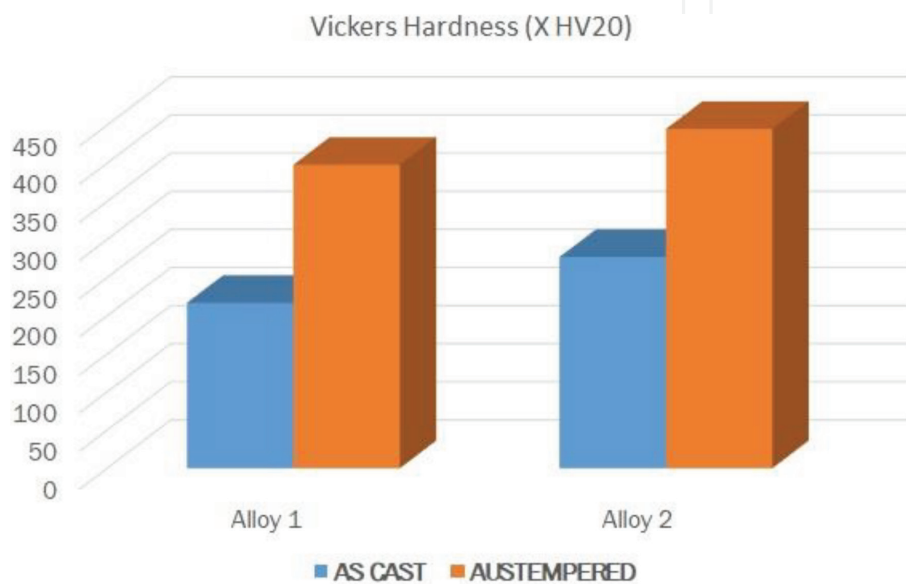


Figure 9.
Vickers hardness for respective as-cast and austempered specimen.

3.2.3 Wear morphology

To understand the wear mechanism involved in due process the worn surfaces for respective as-cast and austempered specimens of both alloys were observed under optical as well as finite element scanning electron microscope and illustrated in **Figures 10** and **11** respectively. The direction of tool travel or wear direction is represented by green arrow for the as-cast and austempered specimens (**Figure 10**). The principal wear mechanism for as-cast and austempered specimens was found to be mostly adhesive wear in nature for all loads. Micro cracks were observed while operating under 10 N for as-cast specimens (**Figure 10(a)**) along with delaminated layer initiated for the soft matrices [45, 46]. Shallow pits and broken wear platelets were also appeared on the surface caused by delamination and work hardening, which was deposited over the graphite nodules. Upon increase in load to 20 N and running for a longer cycles the delaminated layer were observed to be deposited over the graphite nodules (**Figure 10(b)**). The graphite nodules were also observed to expand in transverse direction of wear along with shear deformation [47]. On further increment of load to 30 N (**Figure 10(c)**) the micro cracks were appeared to broaden and surface becomes flat as well as free of wear debris. The wear surface for the austempered specimen under 10 N (**Figure 10(d)**) on the other hand does not have any

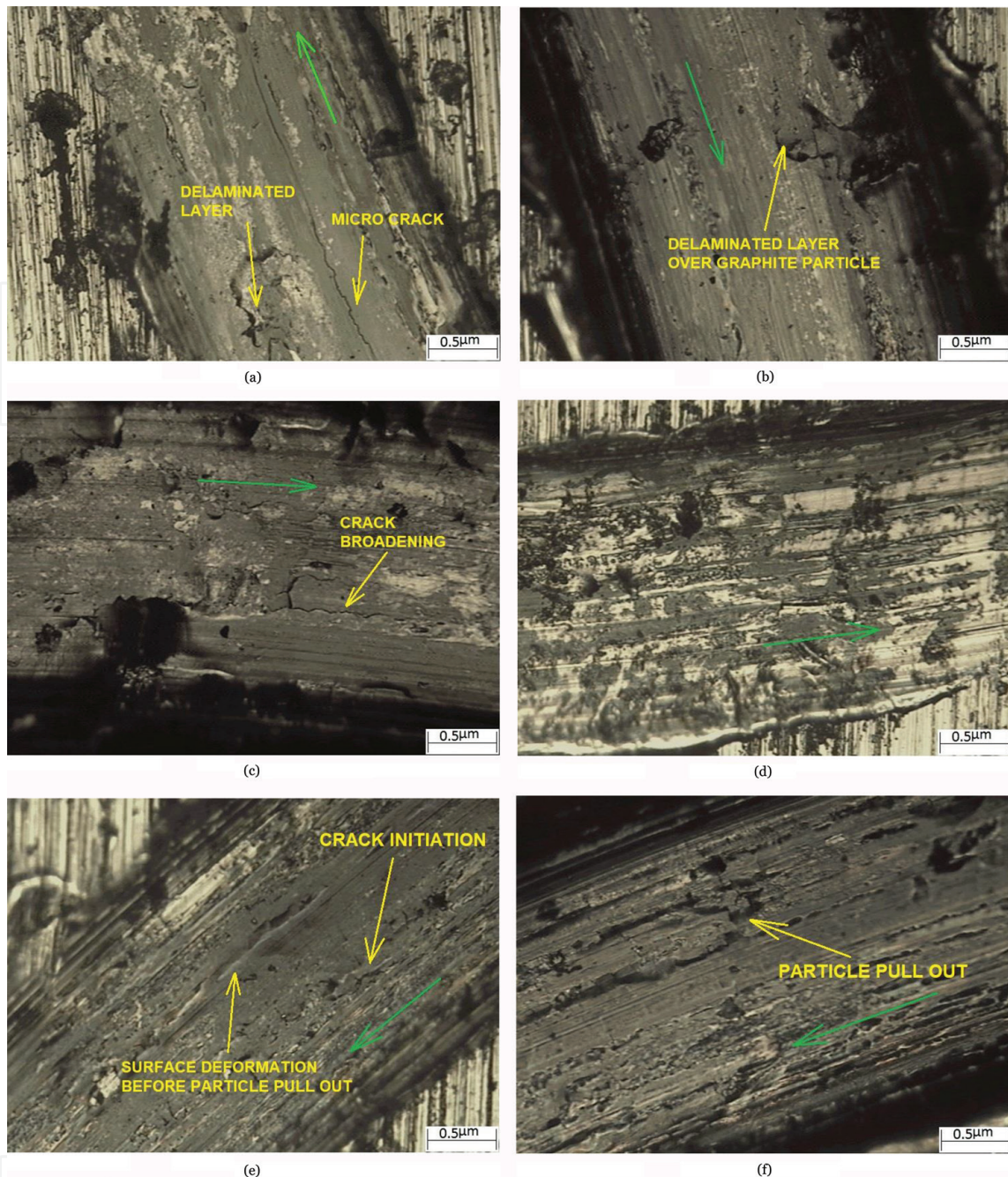


Figure 10. Optical microscopy investigation of worn surface of respective specimen at varying load condition. (a) As-cast specimen under 10 N; (b) as-cast specimen under 20 N; (c) as-cast specimen under 30 N; (d) austempered specimen under 10 N; (e) austempered specimen under 20 N and (f) austempered specimen under 30 N.

cracks formed and appeared to be flat in nature with no specific characteristics. The result can be attributed to the hardness of austempered specimen resulting increased wear resistance and work hardening at an early stage. Upon increase in load to 20 N (**Figure 10(e)**) cracks were initiated at the surface as well as small amount of plastic deformation was observed to be involved that might be due to the attention of plastic stage while running under such high load for a large cycle [48, 49]. The plastic deformed feature was observed to be pulled out (**Figure 10(f)**) of the surface upon continuous frictional effect aroused upon increase in load to 30 N. After such a long run the wear surface does not appear to have any crack on it which is probably due to the particle pull out phenomena resulted through plastic deformation, hence the mechanism involved in this case also classified as adhesive wear.

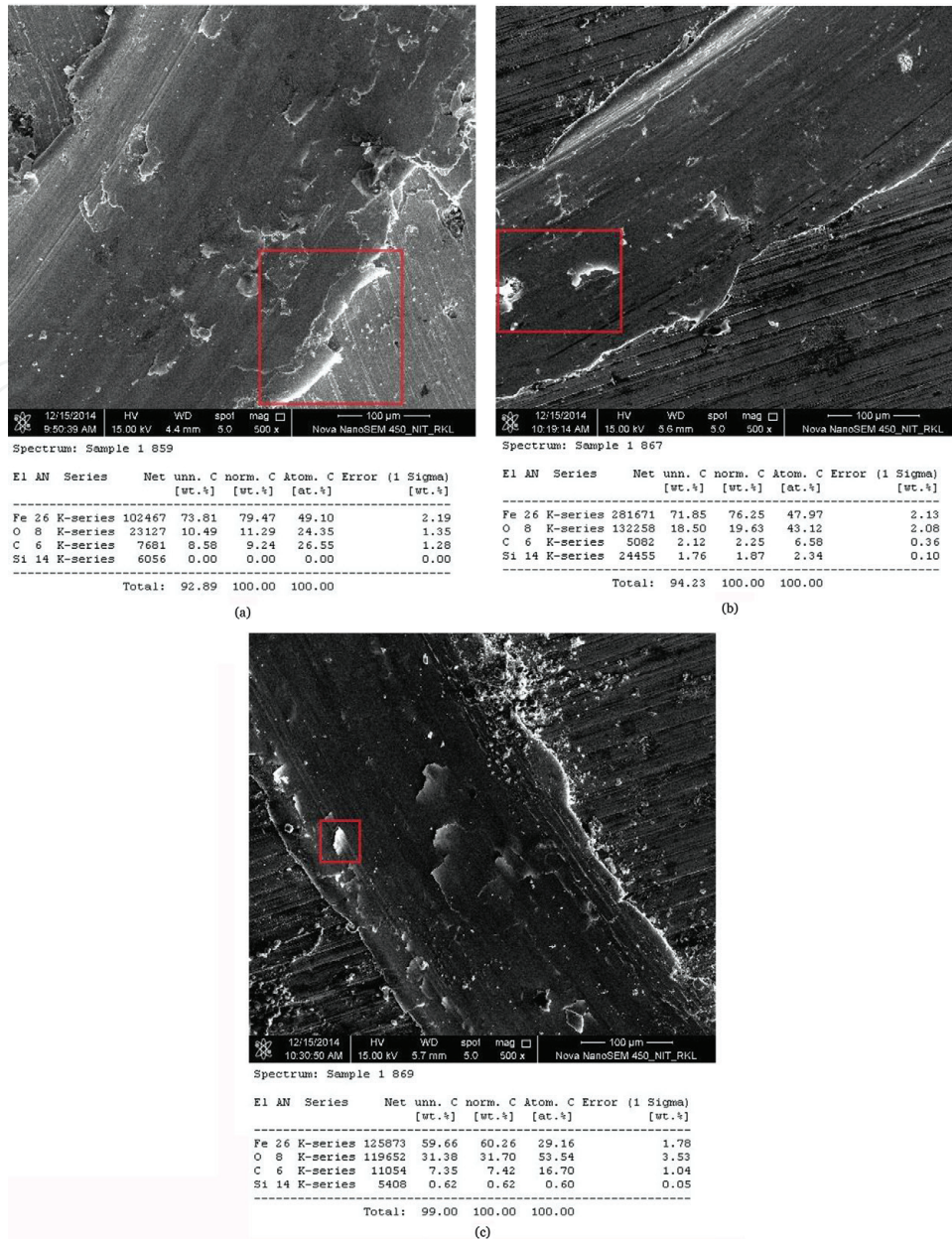


Figure 11. FESEM and EDAX observation for respective specimens with oxide layers. (a) As-cast specimen under 30N, (b) Austempered at 20N load, (c) Austempered at 30N load.

To investigate the presence of any impurity or foreign contamination the worn surfaces of respective specimens were investigated under NOVA NANOSEM 450, field emission scanning electron microscope, with EDAX analysis feature. The as-cast specimens under 10 N and 20 N did not have any significant characteristics on the surface. However at 30 N load the surface appears to have oxide particles present revealed by the FESEM image (**Figure 11(a)**). On the other hand for austempered specimen the oxide particles were observed for both 20 N (**Figure 11(b)**) and 30 N (**Figure 11(c)**). The oxide particles were observed at different places on the wear ring, and that is responsible for the weight gain as observed in the investigation. The respective areas of oxide presence are shown by red rectangles in respective FESEM images along with the EDAX composition analysis at that particular area. The width and depth of wear track was increased with increase in load as well as responsible for reduction in the crack length for respective specimens. The worn surface features are found to be distinctive for 30 N load as compared to 10 and 20 N. The as-cast specimens appeared to have plowing mark at various places and graphite nodules are also observed to start disrupting from their original shape, confirming adhesive wear mechanism. **Figure 12**

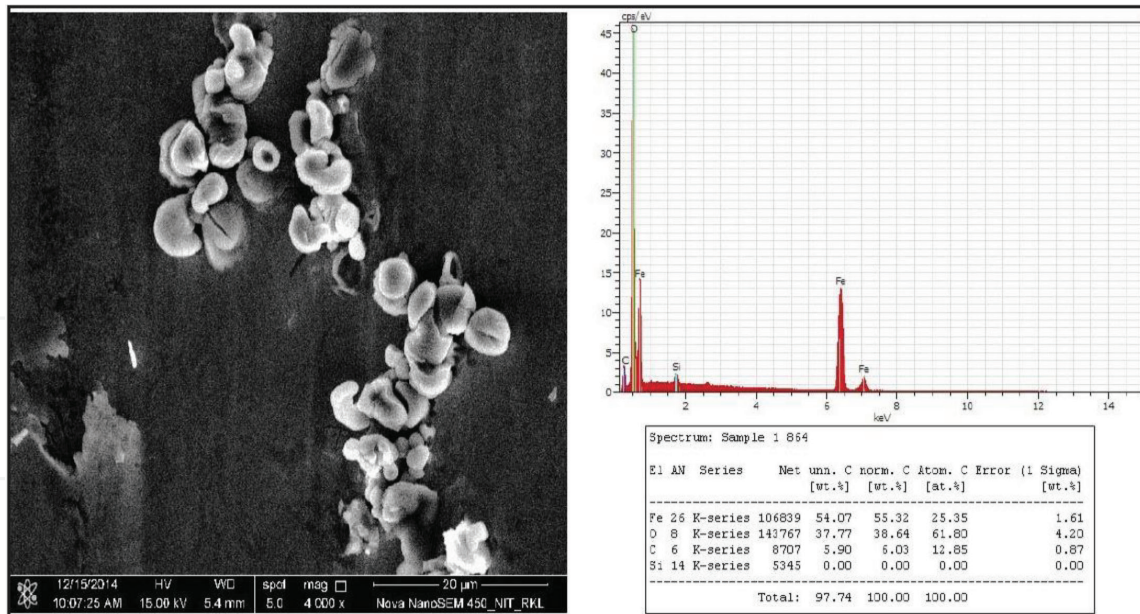


Figure 12.
 EDAX of austempered specimen showing oxides when operated under 30 N load.

depicts the EDAX spectrum of austempered specimen under 30 N load showing the highest peak of oxygen along with Fe.

3.3 Conclusion

The wear behavior of as-cast pearlitic/ferritic ductile iron was compared with upper bainitic austempered specimens with different alloy composition. From investigation the following conclusions can be drawn:

1. Austempering at higher temperature leads to transformation of as-cast ferritic and pearlitic/ferritic matrix for both alloys into coarse upper bainitic matrix and increases the hardness.
2. Soft ferritic matrix was less resistant to wear due to lower level of hardness, whereas austempered coarse upper bainitic matrix with higher hardness value was more resistant to wear.
3. A considerable gain in weight was observed for austempered specimen at 20 N load, whereas the normalized specimen does not show any weight loss or weight gain.
4. Adhesive wear phenomenon was observed for specimens with soft ferritic matrix along with micro cracks due to the hardening of surface while operating under high load and kept on increasing with increase in load.
5. The worn surface when subjected to 10 N load did not show any significant features for austempered specimens, but on the contrary for as-cast soft phase matrices showed plowing micro cracks and delamination features. On the other hand for 30 N loading condition delaminated layer deposition over graphite particles were observed for as-cast specimen and austempered specimen showed particle pull phenomena along with breaking of wear continuity. Under all the loads the wear phenomenon was observed to be adhesive type wear.

Acronyms and abbreviations

SGCI	spheroidal graphite cast iron
DCI	ductile cast iron
ADI	austempered ductile iron

IntechOpen

Author details


Ranjan Kumar Behera^{1*}, Sudipta Sen² and Subash Chandra Mishra²

¹ Accendere Knowledge Management Services Pvt Ltd, New Delhi, India

² Department of Metallurgical and Materials Engineering, National Institute of Technology Rourkela, Rourkela, India

*Address all correspondence to: drranjannitr@gmail.com

IntechOpen

© 2019 The Author(s). Licensee IntechOpen. Distributed under the terms of the Creative Commons Attribution - NonCommercial 4.0 License (<https://creativecommons.org/licenses/by-nc/4.0/>), which permits use, distribution and reproduction for non-commercial purposes, provided the original is properly cited. 

References

- [1] Putatunda SK. Influence of austempering temperature on fracture toughness of a low manganese austempered ductile iron (ADI). *Materials and Manufacturing Processes*. 2001;**16**(2):245-263
- [2] Rebase N, Dommarco R, Sikora J. Wear resistance of high nodule count ductile iron. *Wear*. 2002;**253**(7-8):855-861
- [3] Motu1. Effect of Heat Treatment Procedures on Microstructure and Mechanical Properties of Nodular Iron. 2009. pp. 1-97. Available from: <http://ethesis.nitrkl.ac.in/1501/1/motu-thesis.pdf>
- [4] Abdullah B, Alias SK, Jaffar A, Rashid AA, Ramli A. Mechanical properties and microstructure analysis of 0.5% niobium alloyed ductile iron under austempered process in salt bath treatment. 2010 International Conference on Mechanical and Electrical Technology (ICMET). 2010. pp. 610-614
- [5] Shamanth DS, Murthy KN. Tensile strength and mechanical properties evaluation of permanent mould ductile iron subjected to novel two step austempering process. *International Journal of Engineering Research and Applications (IJERA)*. 2012;**2**(3):2621-2627
- [6] Zammit a, Abela S, Wagner L, Mhaede M, Grech M. Tribological behaviour of shot peened Cu-Ni austempered ductile iron. *Wear*. 2013;**302**(1-2):829-836. Available from: DOI: 10.1016/j.wear.2012.12.027
- [7] Masud L, Martínez R, Simison S, Boeri R. Embrittlement of austempered ductile iron on contact with water-testing under applied potential. *Journal of Materials Science*. 2003;**38**(13):2971-2977
- [8] Elsayed AH, Megahed MM, Sadek AA, Abouelela KM. Fracture toughness characterization of austempered ductile iron produced using both conventional and two-step austempering processes. *Materials and Design*. 2009;**30**(6):1866-1877. Available from: DOI: 10.1016/j.matdes.2008.09.013
- [9] Hsu CH, Chen ML. Corrosion behavior of nickel alloyed and austempered ductile irons in 3.5% sodium chloride. *Corrosion Science*. 2010;**52**(9):2945-2949. DOI: 10.1016/j.corsci.2010.05.006
- [10] Sohi MH, Ahmadabadi MN, Vahdat AB. The role of austempering parameters on the structure and mechanical properties of heavy section ADI. *Journal of Materials Processing Technology*. 2004;**153-154**(1-3):203-208
- [11] Balachandran G, Vadiraj A, Kamaraj M, Kazuya E. Mechanical and wear behavior of alloyed gray cast iron in the quenched and tempered and austempered conditions. *Materials and Design*. 2011;**32**(7):4042-4049. DOI: 10.1016/j.matdes.2011.03.054
- [12] Putatunda SK. Comparison of the mechanical properties of austempered ductile cast iron (ADI) processed by conventional and step-down austempering process. *Materials and Manufacturing Processes*. 2010;**25**(8):749-757. Available from: <http://www.scopus.com/inward/record.url?eid=2-s2.0-77956504093&partnerID=40&md5=c72bebbdefb64febdae0424053023059>
- [13] Krawiec H, Stypuła B, Stoch J, Mikołajczyk M. Corrosion behaviour and structure of the surface layer formed on austempered ductile iron in concentrated sulphuric acid. *Corrosion Science*. 2006;**48**(3):595-607

- [14] Zandira M, Boutorabi SMA. Fracture characteristics of austempered spheroidal graphite aluminum cast irons. *Journal of Iron and Steel Research, International*. 2010;**17**(2):31-35. DOI: 10.1016/S1006-706X(10)60055-6
- [15] Kayali Y, Büyüksağış a, Yalçın Y. Corrosion behavior of boro-tempered ductile iron. *Protection of Metals and Physical Chemistry of Surfaces*. 2010;**46**(3):345-349
- [16] Sugishita J, Fujiyoshi S. The effect of cast iron graphite on friction and wear performance III: The lubricating effect of graphite under rolling-sliding contacts. *Wear*. 1982;**77**(2):181-193. DOI: 10.1016/0043-1648(82)90102-8
- [17] Zimba J, Samandi M, Yu D, Chandra T, Navara E, Simbi DJ. Un-lubricated sliding wear performance of unalloyed austempered ductile iron under high contact stresses. *Materials and Design*. 2004;**25**(5):431-438
- [18] Bai Y, Luan Y, Song N, Kang X, Li D, Li Y. Chemical compositions, microstructure and mechanical properties of roll core used ductile iron in centrifugal casting composite rolls. *Journal of Materials Science and Technology*. 2012;**28**(9):853-858. DOI: 10.1016/S1005-0302(12)60142-X
- [19] Ingole PPM, Awate AU, PSV S. Effect of basic chemical element in sgi (ductile iron). *International Journal of Engineering Research & Technology (IJERT)*. 2012;**1**(7):1-7
- [20] Neri MA, Carreño C. Effect of copper content on the microstructure and mechanical properties of a modified nodular iron. *Materials Characterization*. 2003;**51**(4):219-224. Available from: <http://linkinghub.elsevier.com/retrieve/pii/S1044580303001487>
- [21] Available from: <http://www.ductile.org/didata/Section3/3part2.htm#Manganese Copper Nickel Phosphorus>
- [22] Available from: <http://www.nrc.gov/waste/spent-fuel-storage/diagram-typical-trans-cask-system.doc>
- [23] Available from: http://www.ductile.org/didata/Section2/figures/pfig2_8.htm
- [24] Mochizuki S, Matsushita H. Physical properties of nodular cast iron for shipping containers and safety analysis by fracture mechanics. *Nuclear Engineering and Design*. 1986;**94**(3):309-316
- [25] Droste B. A fracture mechanics safety concept to assess the impact behavior of ductile cast iron containers for shipping and storage of radioactive materials, *Nuclear Engineering and Design*. 1994;**150**:357-366
- [26] Sorenson KB, Salzbrenner RJ. Quality assurance aspects in using ductile cast iron for transportation casks. United States: University of Arizona Nuclear Engineering Dept;1988
- [27] Teng TL, Chu YA, Chang FA, Chin HS, Lee MC. The dynamic analysis of nuclear waste cask under impact loading. *Annals of Nuclear Energy*. 2003;**30**(14):1473-1485
- [28] Jakšić N, Nilsson KF. Finite element modelling of the one meter drop test on a steel bar for the CASTOR cask. *Nuclear Engineering and Design*. 2009;**239**(2):201-213
- [29] Baer W, Bösel D, Eberle A, Klingbeil D. Determination of dynamic crack resistance of ductile cast iron using the compliance ratio key curve method. *Engineering Fracture Mechanics*. 2010;**77**(2):374-384. DOI: 10.1016/j.engfracmech.2009.06.015
- [30] Baer W, Wossidlo P, Abbasi B, Cassau M, Häcker R, Kossert R. Large

scale testing and statistical analysis of dynamic fracture toughness of ductile cast iron. *Engineering Fracture Mechanics*. 2009;**76**(8):1024-1036. DOI: 10.1016/j.engfracmech.2009.01.005

[31] Nilsson KF, Vokál V. Analysis of ductile cast iron tensile tests to relate ductility variation to casting defects and material microstructure. *Materials Science and Engineering A*. 2009;**502**(1-2):54-63

[32] Zencker U, Zeisler P, Droste B. Dynamic fracture mechanics assessments for cubic ductile cast iron containers. *International Journal of Radioactive Materials Transport*. 2000;**11**:113-118

[33] Available from: http://www.ductile.org/didata/Section2/figures/pfig2_5.htm

[34] Uma TR, Simha JB, Murthy KN. Influence of nickel on mechanical and slurry erosive wear behaviour of permanent moulded toughened austempered ductile iron. *Wear*. 2011;**271**(9-10):1378-1384. DOI: 10.1016/j.wear.2010.12.050

[35] Fatahalla N, AbuElEzz A, Semeida M. C, Si and Ni as alloying elements to vary carbon equivalent of austenitic ductile cast iron: Microstructure and mechanical properties. *Materials Science and Engineering A*. 2009;**504**(1-2):81-89. Available from: <http://linkinghub.elsevier.com/retrieve/pii/S0921509308012161>

[36] Zencker U, Weber M, Kovacs O, Qiao L, Droste B. Application limits of low-ductile cast iron. *Proceedings of the 15th International Symposium on the Packaging and Transportation of Radioactive Materials PATRAM 2007* October 21-26. Miami, Florida, USA; 2007. pp. 1-8

[37] Jafar KA, Behnam AA. Influence of mold preheating and silicon content on microstructure and casting properties

of ductile iron in permanent mold. *Journal of Iron and Steel Research, International*. 2011;**18**(3):34-39. DOI: 10.1016/S1006-706X(11)60034-4

[38] Ferro P, Fabrizi a, Cervo R, Carollo C. Effect of inoculant containing rare earth metals and bismuth on microstructure and mechanical properties of heavy-section near-eutectic ductile iron castings. *Journal of Materials Processing Technology*. 2013;**213**(9):1601-1608. DOI: 10.1016/j.jmatprotec.2013.03.012

[39] Choi JO, Kim JY, Choi CO, Kim JK, Rohatgi PK. Effect of rare earth element on microstructure formation and mechanical properties of thin wall ductile iron castings. *Materials Science and Engineering A*. 2004;**383**(2):323-333

[40] Kilicli V, Erdogan M. The nature of the tensile fracture in austempered ductile iron with dual matrix microstructure. *Journal of Materials Engineering and Performance*. 2010;**19**(1):142-149

[41] Cui J, Chen L. Microstructure and abrasive wear resistance of an alloyed ductile iron subjected to deep cryogenic and austempering treatments. *Journal of Materials Science and Technology*. 2017;**33**(12):1549-1554. Available from: <https://linkinghub.elsevier.com/retrieve/pii/S1005030217302086>

[42] Bedolla-Jacuinde A, Guerra FV, Rainforth M, Mejía I, Maldonado C. Sliding wear behavior of austempered ductile iron microalloyed with boron. *Wear*. 2015;**330-331**:23-31. Available from: <https://linkinghub.elsevier.com/retrieve/pii/S0043164815000113>

[43] Zhang H, Wu Y, Li Q, Hong X. Mechanical properties and rolling-sliding wear performance of dual phase austempered ductile iron as potential metro wheel material. *Wear*. 2018; **406-407**:156-165. Available from:

<https://linkinghub.elsevier.com/retrieve/pii/S0043164818300759>

Available from: <https://linkinghub.elsevier.com/retrieve/pii/S2214785318327366>

[44] Polajnar M, Kalin M, Thorbjornsson I, Thorgrimsson JT, Valle N, Botor-Probierz A. Friction and wear performance of functionally graded ductile iron for brake pads. *Wear*. 2017;**382-383**:85-94. Available from: <https://linkinghub.elsevier.com/retrieve/pii/S0043164816308201>

[45] Sun X, Wang Y, Li DY, Wang G. Modification of carbidic austempered ductile iron with nano ceria for improved mechanical properties and abrasive wear resistance. *Wear*. 2013;**301**(1-2):116-121. Available from: <https://linkinghub.elsevier.com/retrieve/pii/S0043164812004462>

[46] Cao HT, Dong XP, Pan Z, Wu XW, Huang QW, Pei YT. Surface alloying of high-vanadium high-speed steel on ductile iron using plasma transferred arc technique: Microstructure and wear properties. *Materials and Design*. 2016;**100**:223-234. Available from: <https://linkinghub.elsevier.com/retrieve/pii/S0264127516303987>

[47] Arabi Jeshvaghani R, Jaberzadeh M, Zohdi H, Shamanian M. Microstructural study and wear behavior of ductile iron surface alloyed by Inconel 617. *Materials and Design*. 2014 Feb;**54**:491-497. Available from: <https://linkinghub.elsevier.com/retrieve/pii/S0261306913008030>

[48] Zhang N, Zhang J, Lu L, Zhang M, Zeng D, Song Q. Wear and friction behavior of austempered ductile iron as railway wheel material. *Materials and Design*. 2016;**89**:815-822. Available from: <https://linkinghub.elsevier.com/retrieve/pii/S0264127515306158>

[49] Samaddar S, Das T, Chowdhury AK, Singh M. Manufacturing of engineering components with austempered ductile iron—A review. *Materials today: Proceedings*. 2018;**5**(11):25615-25624.